

An integrated flow-cell for full sample stream control

G. Hairer · M. J. Vellekoop

Received: 2 December 2008 / Accepted: 12 January 2009 / Published online: 7 March 2009
© Springer-Verlag 2009

Abstract In this study, we present a novel three-dimensional hydrodynamic sheath flow chip that allows full control of a sample stream. The chip offers the possibility to steer each of the four side sheath flows individually. The design of the flow-cell exhibits high flexibility in creating different sample stream profiles (width and height) and allows navigation of the sample stream to every desired position inside the microchannel (vertical and horizontal). This can be used to bring the sample stream to a sensing area for analysis, or to an area of actuation (e.g. for cell sorting). In addition, we studied the creation of very small sample stream diameters. In microchannels (typically $25 \times 40 \mu\text{m}^2$), we created sample stream diameters that were five to ten times smaller than the channel dimensions, and the smallest measured sample stream width was $1.5 \mu\text{m}$. Typical flow rates are $0.5 \mu\text{l}/\text{min}$ for the sample flow and around $100 \mu\text{l}/\text{min}$ for the cumulated sheath flows. The planar microfabricated chip, consisting of a silicon–glass sandwich with an intermediate SU-8 layer, is much smaller ($6 \times 9 \text{mm}^2$) than the previously presented sheath flow devices, which makes it also cost-effective. We present the chip design, fluidic simulation results and experiments, where the size, shape and position of the sample stream have been established by laser scanning confocal microscopy and dye intensity analysis.

Keywords Microfluidics · Three-dimensional hydrodynamic focusing · Numerical simulations · Confocal laser scanning microscope · Dye intensity analysis

1 Introduction

In recent years, microfluidic technology has shown a wide variety of applications in the field of on-chip analysis systems (Stone et al. 2004; DeMello 2006). Microfluidic devices have been utilised for analysis of chemical or biological assays in biochemistry, biophysics, medicine and life sciences (Dittrich et al. 2006). Manipulation of the samples inside the microchannel is an essential aspect for fluidic systems. Therefore, different focusing techniques are used providing the possibility of controlling the passage of the bio-samples or chemical reagents through the microfluidic channels. Advantages are that the channel wall interaction with the sample gets reduced and, in the case of particle analysis, channel clogging can be avoided. Also, a small volume of analytes can be positioned precisely to the region of detection. This sample manipulation finds application in the field of micro-flow cytometry to sort and count cells or particles (Huh et al. 2005), which includes fluorescence-activated cell sorting (FACS) (Wolff et al. 2003; Tung et al. 2004) and Coulter counting (Nieuwenhuis et al. 2004; Rodriguez-Trujillo et al. 2007). In addition, the focusing approach has been applied to a number of different microfluidic applications, including cell patterning (Takayama et al. 1999; Regenberget al. 2004), molecule handling (Lipman et al. 2003; Wang et al. 2008), DNA stretching (Wong et al. 2003), micro-flow switching (Yang et al. 2005b), rapid mixing or dilution (Knight et al. 1998; Lipman et al. 2003; DeMello 2006), bubbles and droplets

G. Hairer (✉) · M. J. Vellekoop
Institute of Sensor and Actuator Systems,
Vienna University of Technology,
Gusshausstr. 27-29,
1040 Vienna, Austria
e-mail: gabriel.hairer@tuwien.ac.at
URL: <http://www.isas.tuwien.ac.at>

generation (Takeuchi et al. 2005; Haeberle et al. 2007), fabrication of monodisperse particles or liposomes (Xu et al. 2005; Huang et al. 2008) and electrospinning of nanofibres (Srivastava et al. 2008).

In literature different focusing approaches have been presented, including electro-kinetic (Shi et al. 2008), dielectrophoretic (DEP) (Yu et al. 2005; Holmes et al. 2006) and hydrodynamic focusing (Knight et al. 1998; Nieuwenhuis et al. 2003; Tsai et al. 2008). The first two techniques are able to focus cells or particles by applying a force field directly to them, which premises certain types of cells or particles; electro-kinetic focusing requires charged species and DEP focusing relies on the polarisation of the particles in the fluid. In the third method mentioned, the hydrodynamic focusing, the sample stream is squeezed by sheath flows. First hydrodynamic focusing devices had a sample flow that was squeezed vertically or horizontally by one or two neighbouring sheath flows. Examples of such an application can be found in Knight et al. (1998) and Simonnet and Groisman (2005). In particle analysis applications, this so called two-dimensional (2D) hydrodynamic focusing technique exhibits the drawback that it does not provide the possibility of single particle analysis even though the focused stream width is of the same order of magnitude as the particles. The particles can be distributed over the total height in the microchannel (see in Fig. 1, left). Further investigations show devices allowing sample focusing in vertical and horizontal directions. This three-dimensional (3D) hydrodynamic focusing technique allows narrowing down the sample stream diameter to the order of the size of the particles and single particle analysis will be possible (see Fig. 1, right). The sample stream can be either hydrodynamically focused on three sides, while at the fourth side the stream moves along the channel bottom (non-coaxial sheath flow), or it can be squeezed on all four sides, where the flow stream flows in the centre of the microchannel (coaxial sheath flow). In both cases, the diameter of the sample stream can be controlled and positioned inside the channel by varying the flow rate ratio between the different sheath flows and the sample flow, as

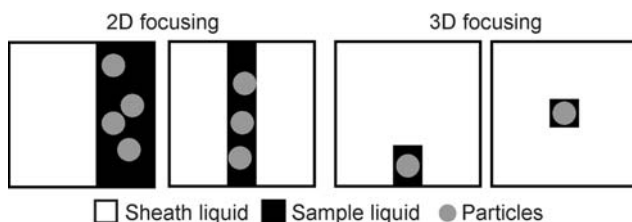


Fig. 1 Schematic of the microchannel cross-section showing four different hydrodynamic focusing types. 2D focusing: one or two sheath flows squeezes the sample stream, 3D focusing: at three (non-coaxial sheath flow) or all four (coaxial sheath flow) sides the sample is focused

shown in Nieuwenhuis et al. (2003). Applications of non-coaxial sheath flow microdevices are Coulter counters, where the sample flow has to be in contact with the measuring electrodes at one channel side (Chung et al. 2003; Scott et al. 2008), and optical detection systems, where the sample stream has to be close to the detection area (Kostner and Vellekoop 2008). Arakawa et al. (2007) uses a non-coaxial sheath flow for particle sorting. Investigations on sample profile characterisations, sample uniformity and focus limitation of non-coaxial sheath flows inside the microchannel have been presented in Hairer et al. (2008).

In recent years, microfluidic devices have been introduced, allowing hydrodynamic focusing by completely surrounding the sample stream with a coaxial sheath flow. Applications of such devices are found in the optical area (Wolff et al. 2003; Holmes et al. 2006). Shoji et al. (2001) fabricated one of the first coaxial sheath flow microdevices using microsystem technology. To realise the vertical sheath flows, a two step introduction of carrier flows was considered and for lateral sheathing the sample inlet was designed smaller than the channel width. Wolff et al. (2003) fabricated a “chimney-like” structure in a microchannel for coaxial sheathing. Sundararajan et al. (2004) fabricated a chip with several PDMS layers using a sandwich technique to achieve a coaxial carrier flow. Later, Yang et al. (2005a) have shown a device using 3D photolithography in SU-8, generating a microchannel to allow 3D sample focusing. Chang et al. (2007) presented a PDMS fabricated scheme, where the sample stream is lifted by an additional inlet forming a coaxial sheath flow, and Mao et al. (2007) introduced the “microfluidic drifting” technique to focus the sample stream. Here, the sample flow drifts to the centre of the microchannel induced by the centrifugal effect in the curve of a microfluidics channel. Sato et al. (2007) reported another way to form passively a coaxial sample flow inside the microchannel. The group realised symmetrically slanted microgrooves at the microchannel walls generating local directional streams, which lifts the sample flow to the centre region of the microchannel. Recently, Tsai et al. (2008) presented a focusing technique where the non-coaxial focused sample stream passes a micro-weir structure for lifting the species. These microfluidic devices are only able to focus the chemical or biological reagents to the central region of the microchannel. Additionally, the channel dimensions of the devices are in the range of 100 μm or even more.

In this paper we present the realisation of a novel three-dimensional hydrodynamic focusing device, which allows creating sample stream dimensions in the range of a few microns and features high versatility. The chip exhibits a number of orthogonal control mechanisms for adjusting the

sample stream dimensions and to navigate it to any position inside the microchannel. Apart from the smaller channel dimensions, the design of the flow-cell exhibits an additional access port compared to that one demonstrated in Hairer et al. (2008), where a sample stream is focused by a non-coaxial sheath flow. The added access port (lifting sheath inlet) features the possibility to form a coaxial sheath flow, allowing full sample stream control inside the microchannel. The idea for such a coaxial fluidic system was firstly published by Nieuwenhuis et al. (2003), who also included initial CFD simulations. In this work, coaxial sheath flow devices have been simulated, fabricated and characterised. The fabricated flow-cell can create an optimal sample stream for several applications (e.g. Coulter counter or FACS). With this device, a sample stream width is achieved featuring a comparable size of, e.g. bacteria and platelets. Additionally, the dimensions of the chip are small ($6 \times 9 \text{ mm}^2$). The major limiting factor for the chip size is that the inlets need an appropriate distance between each other to avoid fluidic short-circuits. For the device, a fluidic interface with a custom-moulded silicone gasket is developed handling narrow inlet distances. The significance of producing smaller flow-focusing devices is that the amount of chips on one wafer is considerably increased (more than 90 chips on one 100 mm-diameter wafer), which results in an important cost reduction, also when integrated sensors will be included. Flow rates between 0.05 and 40 $\mu\text{l}/\text{min}$ are applied at the inlets, which results in a flow velocity between 0.1 and 3 m/s inside the microchannel. For these liquid flow rates and the given channel dimensions, the Reynolds number is between 1 and 50. Therefore, a laminar flow occurs inside the microchannel. The Péclet number, describing the convection/diffusion dispersion, is in the range of 100,000. Such a high Péclet number indicates that convection dominates the transfer and diffusion hardly takes place within the 900 μm -long channel. The laminar flow inside the microchannel with that high Péclet number exhibits an ideal environment for controlling the sample stream. We analysed the fluidic behaviour of the sample stream inside the microchannel using computational fluid dynamic (CFD) simulations and show for the first time experiments of the four-sided coaxial sheath flow control, including confocal laser scanning microscope measurements and dye intensity analysis. These measurements validate the CFD results.

2 Experimental section

2.1 Chip fabrication and description

A photograph of the fabricated device is shown in Fig. 2. The whole chip fabrication and clean room logistics were

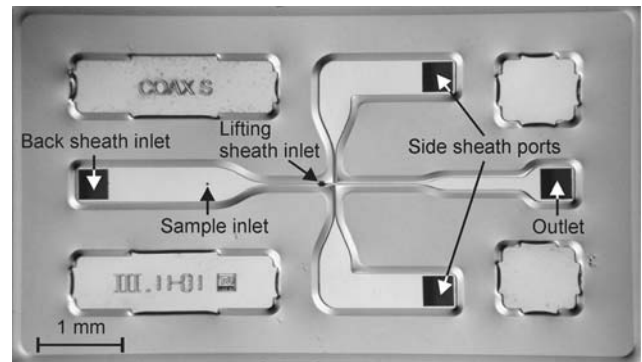


Fig. 2 Photograph of the 3D hydrodynamic focusing sheath flow-cell. Back sheath inlet, side sheath ports and outlet: $330 \times 330 \mu\text{m}^2$; sample inlet: $25 \times 25 \mu\text{m}^2$ and lifting sheath inlet: $25 \times 50 \mu\text{m}^2$; channel dimensions at the channel cross: $25 \times 40 \mu\text{m}^2$ (width \times height)

carried out on 100 mm-diameter wafers. The chip consists of a silicon–glass sandwich with an intermediate layer of SU-8. The access holes for the fluidic interface were anisotropically wet etched in the silicon wafer using a KOH water solution. The silicon wafer has a thickness of 360 μm . As the next step, a 200 μm -thick PYREX glass wafer was coated with the epoxy resist SU-8. The thickness of the SU-8 layer (40 μm) controlled by the spin rate defines the height of the microchannel. The fluidic geometry was generated by structuring the SU-8 layer with standard lithography. To achieve a microfluidic device, the glass wafer including the structured SU-8 layer was thermally irreversibly bonded at 150°C to the silicon wafer (Svasek et al. 2004). Finally, the bonded wafer was diced using a conventional wafer saw.

The resulting hydrodynamic focusing device allows multiple sheath flows. Each sheath flow has its own access port and can be steered individually. The chip has four sheath inlets; three are $330 \times 330 \mu\text{m}^2$ large and the lifting sheath inlet measures $25 \times 50 \mu\text{m}^2$. To compensate the tolerances of the wafer-to-wafer alignment, the size of the lifting sheath inlet in the silicon wafer was designed a little larger ($50 \times 50 \mu\text{m}^2$) and after wafer bonding the inlet achieves the resulting size of $25 \times 50 \mu\text{m}^2$ because of the channel width. The dimensions of the sample inlet are $25 \times 25 \mu\text{m}^2$, and the outlet is $330 \times 330 \mu\text{m}^2$ large. The channel dimensions at the channel cross are 25 μm width and 40 μm height.

In Fig. 3, the principle of the three-dimensional hydrodynamic sheath chip is depicted. The sample liquid is vertically injected into the channel, where a sheath liquid is already flowing from the back (non-coaxial sheath flow). The flow rate ratio between the sample flow and sheath flow defines the sample height in the channel. The sample flow moves along the channel bottom. After a first geometrical focusing section (transversal compression from

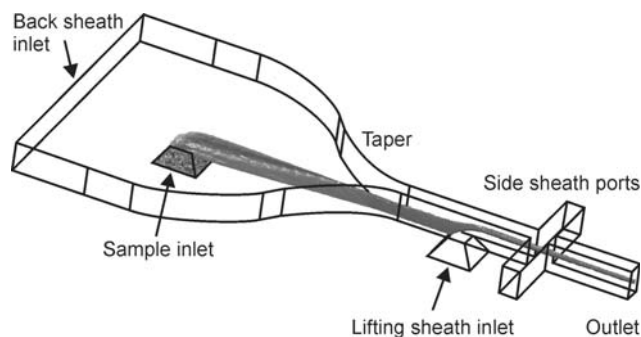


Fig. 3 Schematic of the flow-cell. The sample liquid is vertically injected into the microchannel, where a sheath liquid from the back is already flowing. After a first geometrical focusing step (taper section), the sample stream is lifted and then navigated from the side sheath ports

400 to 25 μm), the sample liquid is lifted by adding sheath liquid through the lifting inlet and a coaxial sheath flow is formed. The additional sheath liquids at the side ports can navigate the sample liquid in the horizontal direction. The sample stream dimensions and its position are controllable by adjusting the flow rates of the sheath inlets and the sample inlet.

2.2 Fluidic connection to the chip

For the hydrodynamic focusing experiments, a fluidic connection to the chip is needed. Therefore, a custom-made plastic holder is fabricated, which includes Teflon tubes to syringes. To combine the chip with the holder, the chip is aligned and glued on an adapted printed circuit board (PCB). This PCB is afterwards mounted on the plastic holder, while a custom-moulded silicone gasket (0.8 mm-thick) is placed between the holder and the fluidic chip to achieve a tight connection. A self-made gasket for tight sealing is needed because the access holes on the chip are very close to each other, which makes the applications of O-rings difficult. In Fig. 4 (bottom right), a cross-section sketch shows the principle. This fluidic connection system has the advantage that at the glass side of the chip near optical measurement can be performed where the microscope objective is directly in contact with the glass of the chip. Figure 4 illustrates details of the fluidic connection and shows the microchip (dimensions: $6 \times 9 \text{ mm}^2$) from the backside with the six access ports.

2.3 Experimental setup

In order to obtain information on the cross-section profiles of the sample stream inside the microchannel, the confocal laser scanning microscope technique (Confocal C1 TE-2000, Nikon, USA) is constituted. The wavelength of the

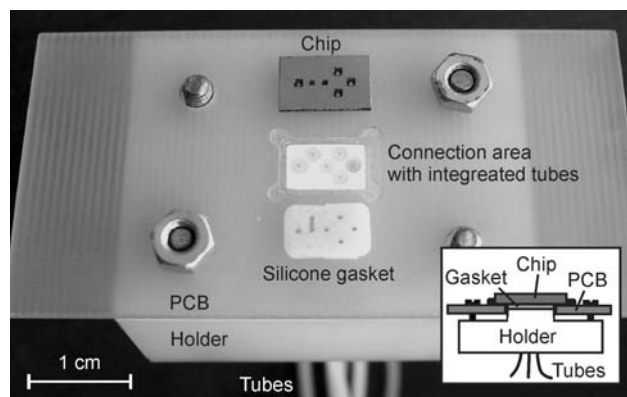


Fig. 4 The holder, PCB, silicone gasket and silicon chip (not assembled yet). Before the PCB is mounted to the holder, the chip is glued on the PCB and the silicone gasket is placed between the holder and the chip. At the bottom right, a cross-section sketch shows the principle

laser amounts to 488 nm and the used filter shows an excitation wavelength spectrum of 450–490 nm and an emission wavelength of 520 nm. This computer-controlled microscope focuses onto a specific horizontal focal plane in the microchannel and scans this area on their fluorescent intensities point-by-point. Repeating the scanning process on several neighbouring channel planes through the total channel height, the measured data are rendered and a 3D image is generated. The resulting pictures give information on the sample stream cross-section (profile) and its position inside the microchannel.

Because dye intensity analysis can be made much faster than confocal microscope measurements, such analysis are carried out using a microscope (Axiotron, Zeiss, Germany) that is coupled to a digital still camera (Cybershot DSC-S75, Sony, Japan). The setup allows capturing vertical images of the device for quantitative sample stream analysis in relation with different applied flow rates at the inlets. However, because of determining the height of the different sheath and sample layers that flow on top of each other, it is also possible to derive three-dimensional information through this method.

For the experiments, the microchip with its fluidic connections is positioned on the scanning area of the (confocal) microscope. The other ends of the Teflon tubes are connected to glass syringes (Hamilton, USA). As sample liquid, the suitable fluorescent dye acridine orange diluted with de-ionised water (concentration: 0.15 mg/ml) is used, and the sheath liquid consists of de-ionised water. The liquids are driven through the device by different volumetric flow rates, which are controlled with syringe pumps (kdScientific model 200 series, USA). In order to prevent the forming of air bubbles, we filled the tubes and the chip with liquid before the chip was mounted on the holder.

3 Numerical simulations

To verify the fluidic behaviour of the sample stream inside the microchannel, numerical simulations are conducted. For the computational fluid dynamic (CFD) simulations, the software tool COMSOL Multiphysics is used. The steady-state flow in the microchannel is governed by the incompressible Navier–Stokes equation, and to visualise the sample stream the coupled convection–diffusion equation with flux is solved. After modelling the geometry of the flow-cell, the physical properties of the sub-domains are defined. As inlet boundary conditions, different flow rates are applied and at the sample inlet a dye concentration is added. The outlet boundary condition is set as neutral with a convective flux. The diffusion coefficient of the diluted fluorescent dye acridine orange in de-ionised water has the value of $3.65 \times 10^{-6} \text{ cm}^2 \text{ s}^{-1}$ (see Pappaert et al. 2005). In order to get a suitable balance between computational solving time and achieving a satisfactory resolution of the numerical result, a mesh of about 100,000 tetrahedral elements for solving the Navier–Stokes equation is generated and approximately 580,000 tetrahedral elements for the convection–diffusion equation. Once the flow fields have been established, the velocity field is substituted into the species of the convection–diffusion equation to calculate the dye concentration field.

4 Results and discussion

4.1 Variety of sample stream profiles and its navigation

Due to the fact that each sheath flow has its own inlet, the chip allows high flexibility in controlling the sample stream (profile and position) inside the channel. The inlets can be either not used (zero flow rates) or exhibit different flow rates, which can also be varied in direction by adding or removing sheath liquid. For the desired sample flow profiles, the corresponding flow rates have to be applied at the inlets. Figure 5 depicts CFD simulation results directly after the side sheath focusing area, showing the possibility of 2D hydrodynamic sample focusing with the microfluidic chip. The images show the dye concentration field in the channel cross-section; black represents the minimum concentration and white the maximum one. In image I, the sample flow is squeezed at one side, where only the left side sheath port is used. Image II shows horizontal sample focusing with two neighbouring side sheath flows (unequal flow rates), and image III highlights vertical sample focusing. To achieve the 2D vertical focusing, liquid has to be removed from the side sheath ports. It can be seen that the confinement of the sample flow in image II is much stronger than in image III. That is not only because of the

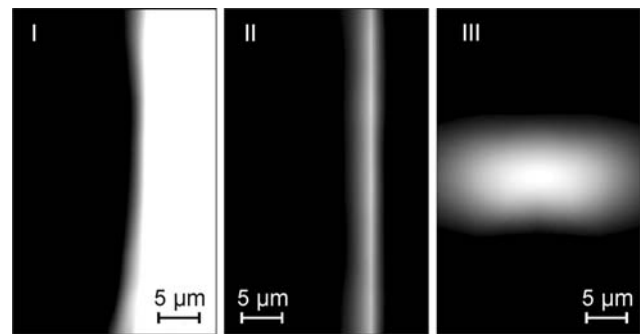


Fig. 5 Simulated 2D hydrodynamic focusing inside the microfluidic device; numerical images of the channel cross-section (directly after the side sheath focusing area) with different sample stream profiles. The sample can be focused with one or two neighbouring sheath flows either horizontally (I and II) or vertically (III). Flow rates ($\mu\text{l}/\text{min}$): back sheath inlet: 1 (I), 1 (II) and 15 (III); sample inlet: 5 (I), 5 (II) and 0.5 (III); lifting sheath inlet: 0 (I), 0 (II) and 12 (III); left side sheath inlet: 10 (I), 10 (II) and -10 (III); right side sheath inlet: 0 (I), 2 (II) and -10 (III)

defined flow rates at the inlets, but also because of the chip design. Due to the geometrical focusing step of the sample stream (see Fig. 3, taper), the back sheath flow does not have the same hydrodynamic focusing power in the vertical direction as the side sheath flows in the horizontal focusing direction. The sample stream profiles shown in image II and III can also be shifted inside the microchannel by adapting the flow rates of the side sheaths, back sheath or lifting sheath ports, respectively.

Figure 6 depicts CFD simulation results showing examples of varied sample profiles at different positions inside the microchannel using the 3D hydrodynamic focusing technique. Note that these images represent the

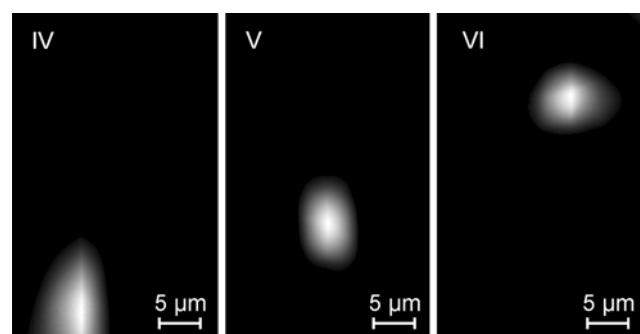


Fig. 6 Simulated 3D hydrodynamic focusing inside the microfluidic device; numerical images of the channel cross-section (directly after the side sheath focusing area) with different sample flow profiles. The sample stream can be focused either to one channel wall (IV) or dynamically controlled inside the channel by adjustable sample diameter (V and VI). Flow rates ($\mu\text{l}/\text{min}$): back sheath inlet: 15 (IV), 20 (V) and 10 (VI); sample inlet: 0.05 (IV), 0.1 (V) and 0.5 (VI); lifting sheath inlet: 0 (IV), 5 (V) and 30 (VI); left side sheath inlet: -8 (IV), 0 (V) and 10 (VI); right side sheath inlet: 5 (IV), 0 (V) and -8 (VI)

situation directly after the side sheath ports in the downstream direction. Image IV shows a non-coaxial focusing of the sample stream, which is shifted a bit to the left-hand side (at the left side sheath port, liquid is removed, and at the right side sheath port, liquid is added). The middle image V shows a lifted sample stream (coaxial sheath flow) and image VI depicts the sample stream positioned at the top right corner. These images show the versatility in sample stream control of the fluidic chip.

4.2 Confocal microscope measurements of the sample stream

In this section, experiments with the confocal microscope are described where the sample stream surrounded by a coaxial sheath flow is measured. Figure 7 shows a three-dimensional confocal image of the sample stream at the channel region where the sample stream is lifted initially and focused afterwards from the sides. The scanning area of the microscope is set to a square of $220 \times 220 \mu\text{m}^2$, which is covered by 512×512 pixels and the vertical step size amounts to $0.5 \mu\text{m}$. This image presents the emitted light of the fluorescent dye. For orientation of the sample stream, the channel geometry is outlined, whereas at the front left corner some lines are left out for better visibility of the sample stream. It can be seen that the sample stream inside the channel is first lifted and then horizontally focused. This image shows that the principle of the coaxial sheathing at all four sides is successful.

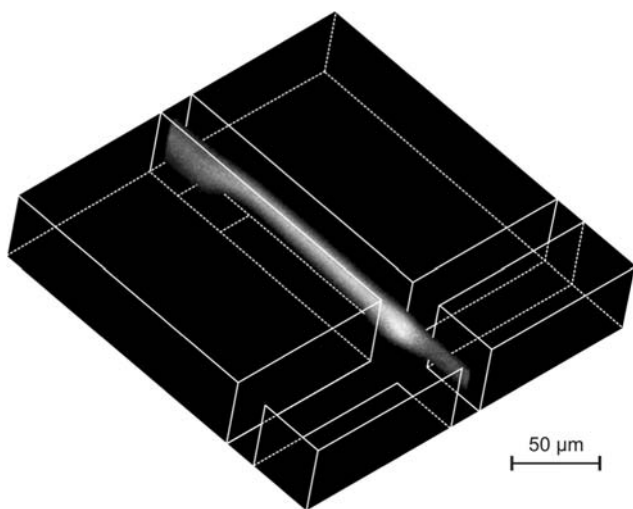


Fig. 7 Measured result with the confocal laser scanning microscope. The sample stream is initially lifted and then squeezed by the flows at the side ports. Flow rates: $15 \mu\text{l}/\text{min}$ (back sheath inlet), $0.5 \mu\text{l}/\text{min}$ (sample inlet), $12.5 \mu\text{l}/\text{min}$ (lifting sheath inlet) and $40 \mu\text{l}/\text{min}$ (side sheath ports). (The edges of the channels are outlined, whereas at the front left corner some lines are left out for better visibility of the sample stream)

As a next step, we analysed the fluidic dynamics of the sample stream and its focusing behaviour. In Fig. 8, top and side views of the sample stream at the lifting and side ports area are shown. The flow rates at the inlet ports were $15 \mu\text{l}/\text{min}$ (back sheath inlet), $0.5 \mu\text{l}/\text{min}$ (sample inlet), $12.5 \mu\text{l}/\text{min}$ (lifting sheath inlet) and $40 \mu\text{l}/\text{min}$ (side sheath inlets). The sample stream is centred to the middle of the channel and additionally horizontally focused. The top view shows that the sample stream broadens a bit after the lifting inlet. This broadening comes from the lifting liquid, pushing the sample to the channel centre. At the channel cross area, the sample stream accumulates a little before it is squeezed. This can also be seen at the side view, where the dye intensity rises. The reason for this sample accumulation is that the flow rates at the side sheath inlets ($2 \times 40 \mu\text{l}/\text{min}$) are fairly high compared to the flow coming from the main channel, where the stream has a flow rate of approximately $28 \mu\text{l}/\text{min}$.

The confocal technology also allows cross-section views, which show the sample flow profile. Figure 9 depicts three channel cross-sections at the region before sample lifting (A), after sample lifting (B) and after side focusing (C). The regions are also depicted in Fig. 8 (top view). Figure 9a shows a non-coaxial sample profile, where the sample moves along the channel bottom. The height of the sample flow reaches approximately one-third of the channel height. After lifting the sample flow, the profile gets somewhat broader in width and its height decreases; see

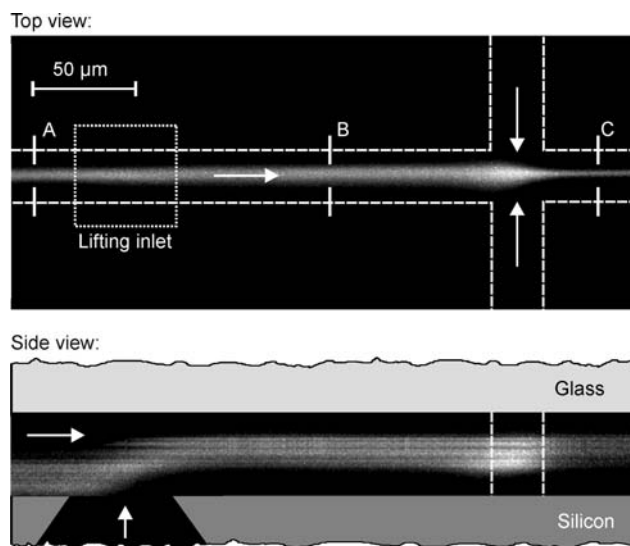


Fig. 8 Measurement result with the confocal laser scanning microscope. *Top* plan view of the section with lifting inlet and side ports. (The edges of the channels are outlined with a dashed line and the lifting inlet in silicon is outlined with a dotted line. The arrows indicate the flow direction). *Bottom* side view of the microchannel. The flow rates at the inlet ports are held at $15 \mu\text{l}/\text{min}$ (back sheath inlet), $0.5 \mu\text{l}/\text{min}$ (sample inlet), $12.5 \mu\text{l}/\text{min}$ (lifting sheath inlet) and $40 \mu\text{l}/\text{min}$ (side sheath inlets)

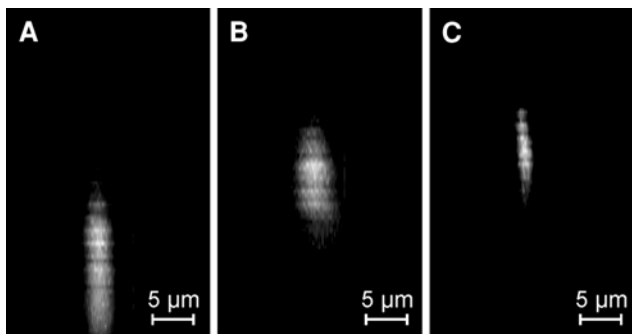


Fig. 9 Confocal measurements inside the microchannel; the pictures reveal from a cross-section perspective the sample flow profiles at the positions *A*, *B* and *C* (Fig. 8, top view)

Fig. 9b. This phenomenon comes from the lifting liquid, which pushes the sample stream up. The size of the sample stream amounts to about one-fifth of the microchannel dimensions. These dimensions of the sample stream will allow focusing single particles of about 6 μm in diameter. In order to test the focusing limit in the horizontal direction, the sample stream is additionally squeezed (40 μl/min at each side port). Figure 9c illustrates the resulting profile; the sample stream is further focused in width, whereas the height of the profile stays almost the same. The minimal measured width amounts to approximately 1.5 μm.

Figure 10 depicts the CFD simulation results of the sample flow profile at the regions *A*, *B* and *C* in Fig. 8 (top view). Here, the same flow rates at the channel inlets are applied as in the presented experiment. These results can be directly compared with the measured ones in Fig. 9. It can be concluded that the simulation results for all three profiles (a, b and c) are in very good agreement with the measurements.

4.3 Dye intensity analysis of the focused sample stream

In this section, we discuss more in detail the resulting sample stream dimensions and its position inside the

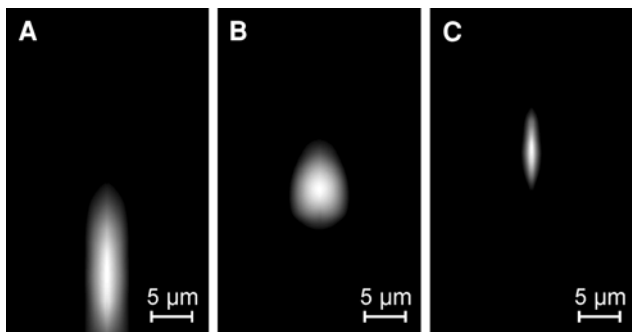


Fig. 10 Simulation results of the flow-cell using the flow rate settings that were applied for the measurements of Fig. 9; the pictures reveal from a cross-section perspective the sample flow profiles at the positions *A*, *B* and *C* (Fig. 8, top view)

microchannel in relation to the applied flow rates at the different channel inlets. The experiments are carried out by dye intensity analyses and the results are compared with CFD simulations.

4.3.1 Vertical control of the sample stream dimensions

A series of measurements were performed in which the vertical dimensions of the sample stream were controlled. First, the penetration of the sample flow into the microchannel was analysed in relation to the flow rate ratio between the back sheath flow and the sample flow. During the experiment, the flow rate of the back sheath flow was kept constant at 15 μl/min, while the sample liquid was injected at different flow rates: 0.05, 0.1, 0.5, 1, 2, 3 and 4 μl/min. The measurements were carried out at the region *A* (Fig. 8, top). At the top of Fig. 11, images of the dye intensity (sample flow) are depicted, showing the intensity change caused by increasing the sample flow rate. These top-viewed images were captured with a digital camera coupled to the microscope. At the left image, the sample flow rate was kept constant at 0.05 μl/min and at the right image at 4 μl/min. For the images in between, the sample

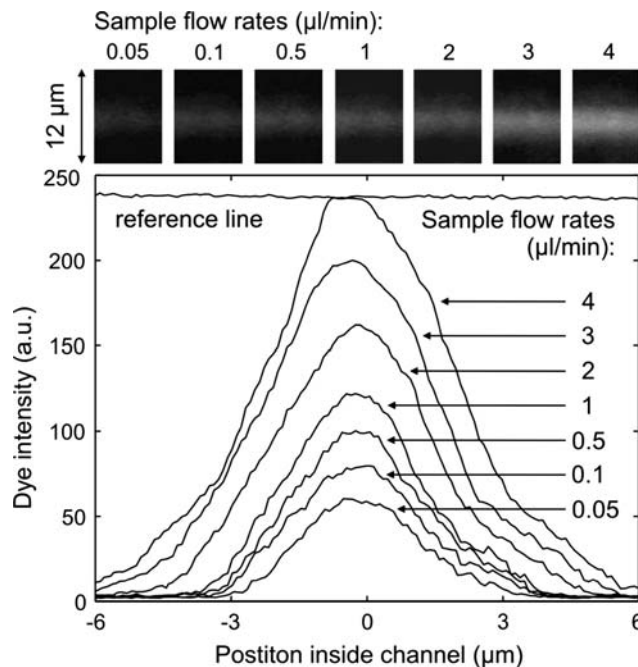


Fig. 11 Top plan-viewed dye intensity images of the sample flow by varying the sample flow rate. The back sheath flow is kept at 15 μl/min. Sample flow rates are according to increase in the dye intensity: 0.05, 0.1, 0.5, 1, 2, 3 and 4 μl/min. The images are a part of the total channel width (25 μm) and the shown channel region is at position *A* (Fig. 8, top view); bottom the different dye intensities of the sample stream over a part of the channel width in relation to the sample flow rates. The reference line depicts the maximum dye intensity, where the channel is fully filled with dye

flow rates that were mentioned before were applied in an upward trend. In Fig. 11 (bottom), the graph shows the different dye intensities of the sample streams over a part at the middle of the channel width. To obtain a reliable result, the intensity of the dye was averaged over 100 adjacent lines. The reference line was achieved by filling the microchannel totally with dye. Under the conditions that the colour intensity of the camera is not in saturation and the absorption of the light in water will be neglected, it can be assumed that this maximum intensity value of the sample represents the height of the microchannel. Therefore, the height of the sample stream inside the microchannel can be calculated by comparing the dye intensity of the sample flow with the reference line. In Hairer et al. (2008), the method for determining the height of the sample stream by intensity analysis is proved with adequate confocal images. The different sample flow heights were calculated by taking the highest intensity value of each curve as shown in Fig. 11. To obtain information on the uncertainty of the measurement results, the same procedure was repeated with additional four images for each sample flow rate. Figure 12 shows the resulting mean value of the different sample flow heights, including the determined error bar. At a sample flow rate of 4 $\mu\text{l}/\text{min}$, the sample flow always reaches the channel ceiling, which results in an error bar of zero. The sample heights resulting from the experiments are additionally compared with CFD simulations. The results show a good match and the sample height inside the channel can be steered between approximately 10 and 40 μm .

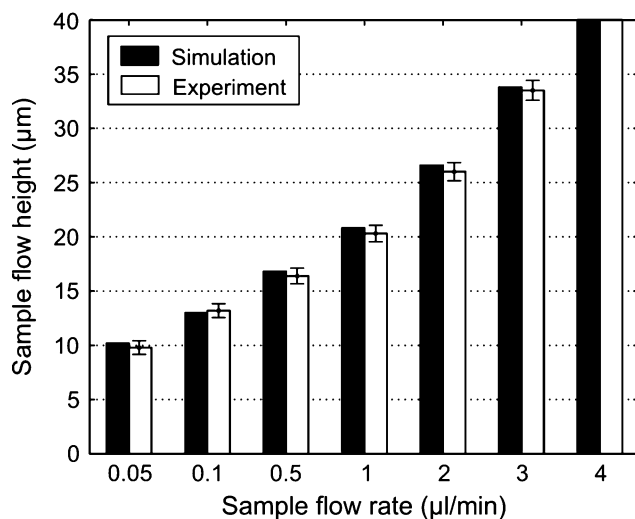


Fig. 12 Comparison of the simulated sample flow height (black bars) inside the microchannel at region A (Fig. 8, top view) and the determined mean value of the sample height (white bars) resulting from five individual dye intensity images; one is shown in Fig. 11. The error bars are additionally included. The back sheath flow is held stable at 15 $\mu\text{l}/\text{min}$

As a next step, the height of the sample lifting inside the microchannel is determined in relation to the flow rate ratio between the lifting sheath flow and the combination of the back sheath flow and sample flow. During this experiment, the back sheath flow and the sample flow were kept constant (15 $\mu\text{l}/\text{min}$ at the back sheath inlet and 0.5 $\mu\text{l}/\text{min}$ at the sample inlet). At these flow conditions, the sample flow height is about one-third of the channel height (see Fig. 12, or for the sample profile see Fig. 9a). The lifting sheath flow rate was varied from 1 to 16 $\mu\text{l}/\text{min}$ (see Fig. 13). In order to measure the height of sample lifting, the dye was not injected at the sample inlet, but at the sheath lifting inlet. Dye intensity analyses were carried out the same way as discussed in the previous paragraph. The images were taken at the region B (Fig. 8, top). From the achieved intensity images of the lifting sheath flow, the height of the lifting flow (equivalent to the sample lifting height) was calculated. Figure 13 (bottom) shows the results of the experiment (mean value of height and error bar based on five images with the same flow conditions) and the corresponding CFD simulations, which are in good agreement. At a sheath lifting flow rate of 1 $\mu\text{l}/\text{min}$, the sample stream is lifted to about 4 μm from the channel bottom. By increasing the sheath lifting flow rate, the sample stream is

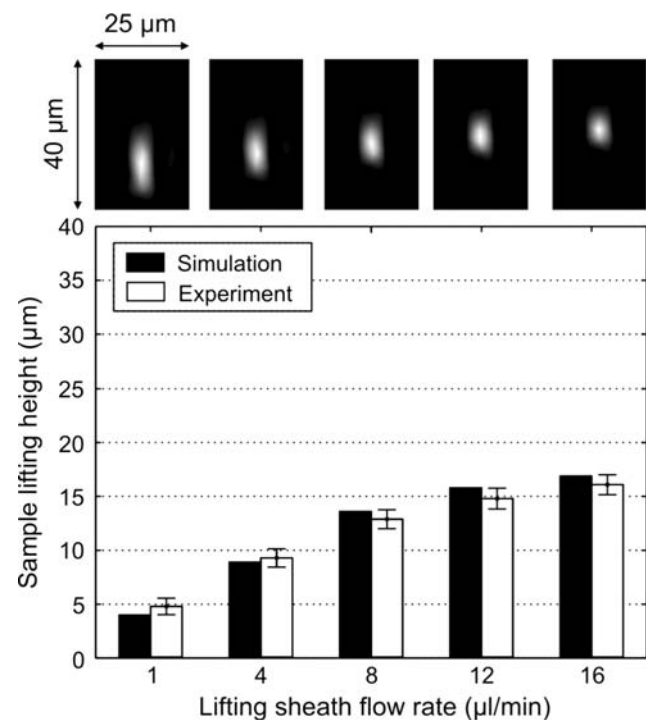


Fig. 13 Top simulated cross-section view of the sample stream in relation to different lifting sheath flow rates; bottom comparison of the simulated sample lifting height (black bars) inside the microchannel at region B (Fig. 8, top view) and the determined mean value of the sample lifting height (white bars) resulting from dye intensity analysis (data not shown). The back sheath flow is held stable at 15 $\mu\text{l}/\text{min}$ and the sample flow at 0.5 $\mu\text{l}/\text{min}$

lifted further to the channel centre. For sheath lifting flow rates higher than 12 $\mu\text{l}/\text{min}$, the sample lifting does not change much anymore with these flow conditions. If the sample stream has to be shifted further to the channel ceiling, the flow rate of the back sheath inlet has to be reduced (see Fig. 6, VI). Figure 13 (top) depicts CFD simulation images of the sample stream profile in a cross-view perspective, which correspond to the lifting sheath flow rate shown beneath. The image series shows that if the flow rate of the lifting sheath inlet is increased, the sample stream will not only be lifted to the centre of the microchannel, but it will also be squeezed in a vertical direction. For achieving the desired sample stream height at a defined sample lifting place inside the microchannel, all three flow rates form the back sheath inlet, the sample inlet and the lifting sheath inlet have to be taken into account. It can be concluded that the above shows the high flexibility of the device in controlling the sample lifting height.

4.3.2 Horizontal control of the sample stream dimensions

Beside the experiments for the vertical control of the sample flow, additionally a series of measurements were carried out to analyse the horizontal control of the sample stream, where the width of the sample flow and the sample flow shifting steered by the side sheath ports were analysed. During the experiment, the flow rates at the back sheath inlet, sample inlet and the lifting sheath inlet were kept constant at 15, 0.5 and 12.5 $\mu\text{l}/\text{min}$, respectively. For these flow conditions, the sample stream is surrounded by a coaxial sheath flow and the sample stream flows in the centre of the microchannel. The sample stream exhibits a size of about 6 μm in diameter, as shown in Fig. 9b. The flow rates at the side sheath ports were varied to control the width of the sample stream and its flow position in the horizontal direction. At the side sheath ports, liquid was either added or removed. If liquid is removed we call the flow rate negative. For the experiments, images were taken with the digital camera at the area of the side sheath ports. The dye intensity of the sample stream was analysed at the region C shown in Fig. 8 (top).

In a first step, the width of the sample stream was controlled, where the same flow rate at both side sheath ports were applied and varied in the range from -10 to 40 $\mu\text{l}/\text{min}$. Figure 14 shows the determined sample width over the different flow rates of the side sheath ports, which can be controlled over a wide range. Each depicted sample width represents the mean value of the sample widths derived from five images under the same flow conditions. The resulting error bars are additionally included. At negative side sheath flow rates, the sample width responds very sensitive to flow rate changes at the side sheath ports, which leaks in measurement accuracy. At a flow rate of

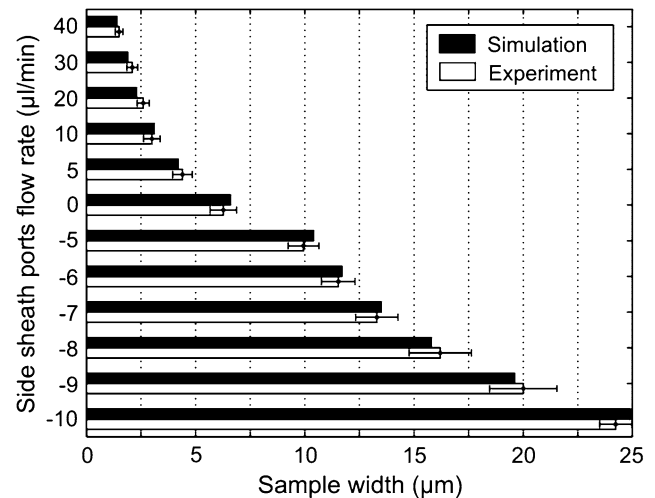


Fig. 14 Comparison of the simulated sample flow width (black bars) inside the channel at region C (Fig. 8, top view) and the determined mean value of the sample width (white bars) resulting from its dye intensity analysis (data not shown). Other flow rates: 15 $\mu\text{l}/\text{min}$ (back sheath flow), 0.5 $\mu\text{l}/\text{min}$ (sample flow) and 12.5 $\mu\text{l}/\text{min}$ (lifting sheath flow)

-10 $\mu\text{l}/\text{min}$ at both the side ports, the sample stream is enlarged to the channel width of 25 μm . This flow rate is also the limit where still no sample liquid is flowing into the side ports, which will occur if more liquid is removed from the side ports. By adding sheath liquid through the side ports, the sample stream is squeezed horizontally. At the flow rate of 40 $\mu\text{l}/\text{min}$ at both side ports, the sample width amounts to approximately 1.5 μm . The resulting sample profile is shown in Fig. 9c. This width exhibits the horizontal focusing limit of the flow-cell. Further decrease of the sample flow width appeared not possible, because the flow rates between sample and sheath flows became so large that the regular sample flow was disturbed and not visible any more.

Finally, the horizontal sample flow positioning in relation to the applied flow rates at the side ports was analysed. The flow rates for the other inlets (back sheath, sample and lifting sheath) were kept constant at the values mentioned before, where the sample stream exhibits the profile as shown in Fig. 9b. To shift the sample stream inside the microchannel, the sheath liquid flow at the side sheath ports were applied in the opposite direction. Figure 15 shows images at the side ports area with different applied flow rates at the side ports. On the left-hand side, some illustrative top-viewed images of the experimental results are depicted, and at the right-hand side, the corresponding CFD simulations in a cross-section perspective are shown. The simulated images show the sample profile directly after the side ports in the flow direction, and they illustrate where the sample stream flows inside the microchannel. The horizontal control of the sample flow dimension shows

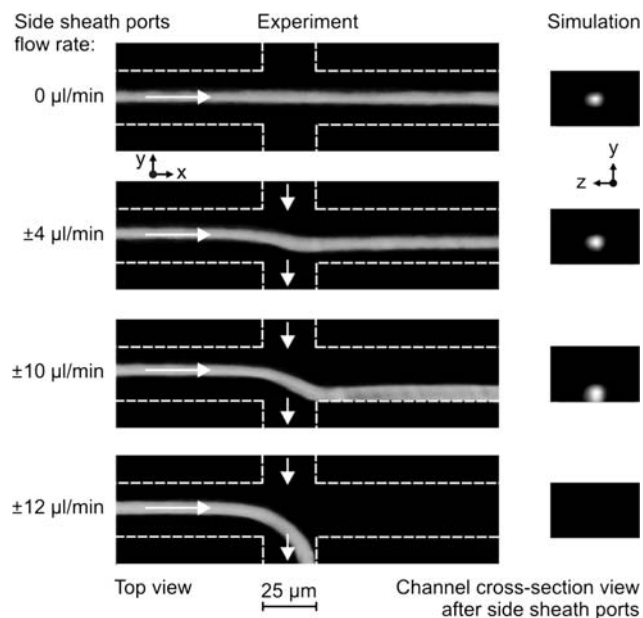


Fig. 15 *Left* measured images of the sample stream at the side ports area in relation to the flow rates at the sheath side ports (the channel edges are outlined with a dashed line. The arrows indicate the flow direction); *right* corresponding simulated results after the side ports in the flow direction. Other flow rates: 15 $\mu\text{l}/\text{min}$ (back sheath flow), 0.5 $\mu\text{l}/\text{min}$ (sample flow) and 12.5 $\mu\text{l}/\text{min}$ (lifting sheath flow)

a good match between experimental results and the CFD simulations. By increasing the flow rates at both side ports, the sample stream is shifted to one channel side wall, whereas the sample stream diameter stays almost the same. At flow rates of $\pm 10 \mu\text{l}/\text{min}$, the sample stream flows along the channel wall. If the flow rates are even further increased, the sample stream starts to split up and a part of the flow runs through one side sheath port. At the flow rates of $\pm 12 \mu\text{l}/\text{min}$, the sample stream completely flows through one side channel, as shown in Fig. 15 (bottom). The flow rates can be further increased so that the sample stream does not even touch any channel wall.

Figure 16 shows the quantitative results of the horizontal sample flow shifting for the presented images in Fig. 15, where 100 adjacent lines of the dye intensity were averaged to obtain reliable results. The dye intensity stays the same and the sample width hardly changes. It becomes only a little bit broader when the sample stream is shifted to the channel wall side. If the flow rates at the side sheath ports are not only applied in opposite direction, but also exhibit absolute different flow rates, the width of the horizontal shifted sample stream can additionally be varied (focused or expanded). These examples emphasise the versatility of the flow-cell.

In combination with (integrated) sensors, this microfluidic device is suitable for on-chip flow cytometry to analyse single cells. Even more, it allows the integration of electrodes for a Coulter counter at the non-coaxial sheath

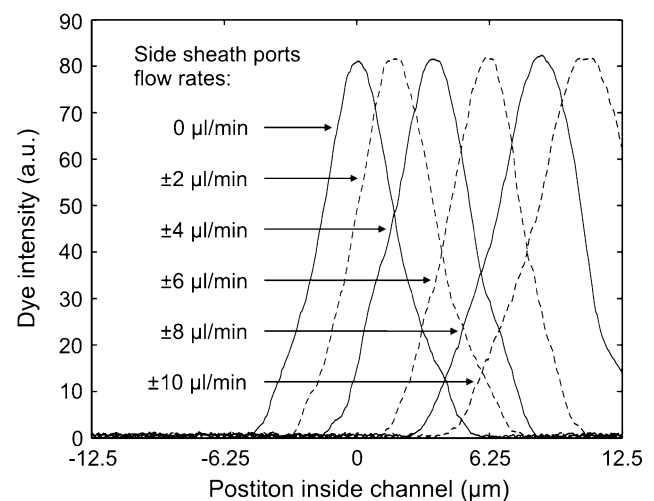


Fig. 16 Dye intensity of the sample stream over the channel width in relation to the flow rates at the side sheath ports at region C (Fig. 8, top view). At one side sheath port, liquid is added, whereas at the other liquid is removed with the same flow rate. The sample stream moves to the right-hand side. Flow rates: 15 $\mu\text{l}/\text{min}$ (back sheath flow), 0.5 $\mu\text{l}/\text{min}$ (sample flow) and 12.5 $\mu\text{l}/\text{min}$ (lifting sheath flow)

flow region or mounting of glass fibres for FACS at the coaxial sheath flow to form a complete integrated analysis system. Another possibility would be to use the flow-cell in cell sorting applications.

5 Conclusions

We have developed a microfabricated flow-cell that is very versatile in sample stream focusing. Due to the fact that each of all four sheath flow sides can be individually steered, the flow-cell can not only adjust the sample stream profile and its dimensions, but it can also freely position the sample stream inside the microchannel. CFD simulations confirm the flexible sample stream control. The flow-cell allows hydrodynamic focusing of the sample stream either in two or in three dimensions. It can also generate non-coaxial and coaxial sheath flows in different parts of the channel. Experiments have been carried out using a confocal laser scanning microscope, where the generated sample flow profiles were characterised. Additionally, intensity analyses of the sample stream in relation to the applied flow rates at all inlets were made to establish the resulting sample stream size and its position inside the microchannel. These results were compared with the numerical simulations showing that the complicated flow behaviour of the flow-cell can be accurately modelled. The flow-cell allows the forming of very small sample streams. In the horizontal direction, we achieved a sample width of approximately 1.5 μm , and in the vertical direction this was about 8 μm . This microfluidic device allows precise focusing and positioning of molecules or particles inside

the microchannel. The advantages of this microfluidic system are the possibility to steer the sample flow to optimal analysis positions in the channel (e.g. in the focal point of an optical sensor or to the channel bottom where measurement electrodes are located) and the control of the coaxial sample flow diameter, allowing the lineup of single cells in the channel and enhancing single cell analysis.

Acknowledgments The authors would like to thank the University Service Centre for Transmission Electron Microscopy (USTEM) at the Vienna University of Technology for providing the possibility to make the confocal laser scanning microscope measurements. We also acknowledge our colleagues from the Sensor Technology Lab (Institute of Sensor and Actuator Systems, Vienna University of Technology), especially G. Pärri, P. Svasek, E. Pirker and Dr. A. Jachimowicz, for fruitful discussions and the fabrication of the devices, the chip-holder and the custom-built mould.

References

- Arakawa T, Shirasaki Y, Aoki T, Funatsu T, Shoji S (2007) Three-dimensional sheath flow sorting microsystem using thermosensitive hydrogel. *Sens Actuators A* 135:99–105
- Chang C-C, Huang Z-X, Yang R-J (2007) Three-dimensional hydrodynamic focusing in two-layer polydimethylsiloxane (PDMS) microchannels. *J. Micromech Microeng* 17:1479–1486
- Chung S, Park SJ, Kim JK, Chung C, Han DC, Chang JK (2003) Plastic microchip flow cytometer based on 2- and 3-dimensional hydrodynamic flow focusing. *Microsyst Technol* 9:525–533
- DeMello AJ (2006) Control and detection of chemical reactions in microfluidic systems. *Nature* 442:394–402
- Dittrich PS, Tachikawa K, Manz A (2006) Micro total analysis systems. Latest advancements and trends. *Anal Chem* 78:3887–3907
- Haerberle S, Zengerle R, Duerce J (2007) Centrifugal generation and manipulation of droplet emulsions. *Microfluid Nanofluid* 3:65–75
- Hairer G, Pärri GS, Svasek P, Jachimowicz A, Vellekoop MJ (2008) Investigations of micrometer sample stream profiles in a three-dimensional hydrodynamic focusing device. *Sens Actuators B* 132:518–524
- Holmes D, Morgan H, Green NG (2006) High throughput particle analysis: combining dielectrophoretic particle focussing with confocal optical detection. *Biosens Bioelectron* 21:1621–1630
- Huang SH, Khoo HS, ChangChien SY, Tseng FG (2008) Synthesis of bio-functionalized copolymer particles bearing carboxyl groups via a microfluidic device. *Microfluid Nanofluid* 5:459–468
- Huh D, Gu W, Kamotani Y, Grotberg JB, Takayama S (2005) Microfluidics for flow cytometric analysis of cells and particles. *Physiol Meas* 26:R73–R98
- Knight JB, Vishwanath A, Brody JP, Austin RH (1998) Hydrodynamic focusing on a silicon chip: mixing nanoliters in microseconds. *Phys Rev Lett* 80:3863–3866
- Kostner S, Vellekoop MJ (2008) Cell analysis in a microfluidic cytometer applying a DVD pickup head. *Sens Actuators B* 132:512–517
- Lipman EA, Schuler B, Bakajin O, Eaton WA (2003) Single-molecule measurements of protein folding kinetics. *Science* 301:1233–1235
- Mao X, Waldeisen JR, Huang TJ (2007) “Microfluidic drifting”-implementing three-dimensional hydrodynamic focusing with a single-layer planar microfluidic device. *Lab Chip* 7:1260–1262
- Nieuwenhuis JH, Bastemeijer J, Sarro PM, Vellekoop MJ (2003) Integrated flow-cells for novel adjustable sheath flows. *Lab Chip* 3:56–61
- Nieuwenhuis JH, Kohl F, Bastemeijer J, Sarro PM, Vellekoop MJ (2004) Integrated Coulter counter based on 2-dimensional liquid aperture control. *Sens Actuators B* 102:44–50
- Pappaert K, Biesemans J, Clicq D, Vankrunkelsven S, Desmet G (2005) Measurements of diffusion coefficients in 1-D micro- and nanochannels using shear-driven flows. *Lab Chip* 5:1104–1110
- Regenberg B, Kruhne U, Beyer M, Pedersen L, Simon M, Thomas O, Nielsen J, Ahl T (2004) Use of laminar flow patterning for miniaturised biochemical assays. *Lab Chip* 4:654–657
- Rodriguez-Trujillo R, Mills CA, Samitier J, Gomila G (2007) Low cost micro-Coulter counter with hydrodynamic focusing. *Microfluid Nanofluid* 3:171–176
- Sato H, Sasamoto Y, Yagyu D, Sekiguchi T, Shoji S (2007) 3D sheath flow using hydrodynamic position control of the sample flow. *J Micromech Microeng* 17:2211–2216
- Scott R, Sethu P, Harnett CK (2008) Three-dimensional hydrodynamic focusing in a microfluidic Coulter counter. *Rev Sci Instrum* 79:046104
- Shi J, Mao X, Ahmed D, Colletti A, Huang TJ (2008) Focusing microparticles in a microfluidic channel with standing surface acoustic waves (SSAW). *Lab Chip* 8:221–223
- Shoji S, Akahori K, Tashiro K, Sato H, Honda N (2001) Design and fabrication of micromachined chemical/biochemical systems. *Focused Sci Technol Micro/Nano Scale* 36:8–11
- Simonnet C, Groisman A (2005) Two-dimensional hydrodynamic focusing in a simple microfluidic device. *Appl Phys Lett* 87:114104
- Srivastava Y, Rhodes C, Marquez M, Thorsen T (2008) Electrospinning hollow and core/sheath nanofibers using hydrodynamic flow focusing. *Microfluid Nanofluid* 5:455–458
- Stone HA, Stroock AD, Ajdari A (2004) Engineering flows in small devices: microfluidics towards a lab-on-a-chip. *Annu Rev Fluid Mech* 36:381–411
- Sundararajan N, Pio MS, Lee LP, Berlin AA (2004) Three-dimensional hydrodynamic focusing in polydimethylsiloxane (PDMS) microchannels. *J Microelectromech Syst* 13:559–567
- Svasek P, Svasek E, Lendl B, Vellekoop MJ (2004) Fabrication of miniaturized fluidic devices using SU-8-based lithography and low temperature wafer bonding. *Sens Actuator A* 115:591–599
- Takayama S, McDonald JC, Ostuni E, Liang MN, Kenis PJA, Ismagilov RF, Whitesides GM (1999) Patterning cells and their environments using multiple laminar fluid flows in capillary networks. *Proc Natl Acad Sci* 96:5545–5548
- Takeuchi S, Garstecki P, Weibel DB, Whitesides GM (2005) An axisymmetric flow-focusing microfluidics device. *Adv Mater* 17:1067–1072
- Tsai C-H, Hou H-H, Fu L-M (2008) An optimal three-dimensional focusing technique for micro-flow cytometers. *Microfluid Nanofluid* 5:827–836
- Tung Y-C, Zhang M, Lin C-T, Kurabayashi K, Skerlos SJ (2004) PDMS-based opto-fluidic micro-flow cytometer with two-color, multi-angle fluorescence detection capability using PIN photodiodes. *Sens Actuators B* 98:356–367
- Wang F, Wang H, Wang J, Wang H-Y, Rummel PL, Garimella SV, Lu C (2008) Microfluidic delivery of small molecules into mammalian cells based on hydrodynamic focusing. *Biotechnol Bioeng* 100:150–158
- Wolff A, Perch-Nielsen IR, Larsen UD, Friis P, Goranovic G, Poulsen CR, Kutter JP, Telleman P (2003) Integrating advanced functionality in a microfabricated high-throughput fluorescent-activated cell sorter. *Lab Chip* 3:22–27
- Wong PK, Lee Y-K, Ho C-M (2003) Deformation of DNA molecules by hydrodynamic focusing. *J Fluid Mech* 497:55–65

- Xu S, Nie S, Seo M, Lewis P, Kumacheva E, Stone H, Garstecki P, Weibel D, Gitlin I, Whitesides GM (2005) Generation of monodisperse particles by using microfluidics: control over size, shape and composition. *Angew Chem Int Ed* 44:724–728
- Yang R, Feedback DL, Wang W (2005a) Microfabrication and test of a three-dimensional polymer hydro-focusing unit for flow cytometry applications. *Sens Actuators A* 118:259–267
- Yang R-J, Chang C-C, Huang S-B, Lee G-B (2005b) A new focusing model and switching approach for electrokinetic flow inside the microchannel. *J. Micromech Microeng* 5:2141–2148
- Yu C, Vykoukal J, Vykoukal DM, Schwartz JA, Shi L, Gascoyne PRC (2005) A three-dimensional dielectrophoretic particle focusing channel for microcytometry application. *J Microelectromech Syst* 14:480–487